Comparison of LGE MRI Scar Identification Methods for Atrial Computational Modeling

Jake A Bergquist[1,2,3], Benjamin Orkild[1,2,3], Eugene Kwan[2], Karli Gillette[1,3], Kyoichiro Yazaki[2], Surachat Jaroonpipatkul[2], Ed Dibella[4], Rich Shelton[5], Erik Beiging[5], Lowell Chang[5], Gernot Plank[6], Shireen Elhabian,[1] Rob S MacLeod[1,2,3], Ravi Ranjan[2,3,5],

[1] Scientific Computing and Imaging Institute, University of Utah, SLC, UT, USA
[2] Nora Eccles Cardiovascular Research and Training Institute, University of Utah, SLC, UT, USA
[3] Department of Biomedical Engineering, University of Utah, SLC, UT, USA
[4] Department of Radiology & Imaging Sciences, University of Utah, SLC, UT, USA
[5] Veteran's Affairs, University of Utah, SLC, UT, USA
[6] Division of Biophysics and Medical Physics, Gottfried Schatz Research Center, Medical University of Graz, Austria

Abstract

Identification of patient-specific scar and fibrosis is a critical step in the personalization of cardiac computational models. Late gadolinium enhanced cardiac magnetic resonance imaging (LGE-cMRI) is often used to identify patient anatomy, as well as tissue fibrosis and scar. Automated methods to identify scar from LGE-cMRI exist. Still, there is no clear consensus as to which is best in the context of patient-specific computational modeling of atrial fibrillation. There has been no substantial investigation into the effects that variability in scar may have on downstream patient-specific simulations. This study compares the distribution of scar patterns generated via automated LGE-cMRI analysis alongside human-guided scar identification. We assess the effects each identified scar pattern has on downstream computational modeling outputs by comparing the number of stable re-entrant arrhythmias induced In Silico in atrial fibrillation. We find both substantial disagreement between scar patterns identified via automated and human-guided methods, as well as sensitivity in the arrhythmia simulation outcomes across scar patterns. These results highlight the sensitivity of such computational models to these input parameters and enforce the need for robust personalization tools in the cardiac modeling field.

1. Introduction

Identification of cardiac tissue properties from late gadolinium enhanced cardiac magnetic resonance imaging (LGE-cMRI) is an established field of study that is heavily leveraged in the formulation of cardiac computational models.[1, 2] Several methods exist to set LGE-cMRI thresholds for identifying tissue properties such as scar automatically.[3–6] It is imperative to understand how differences in these upstream decisions–what LGE threshold to use when building a model–affect downstream outputs such as simulations of arrhythmogenesis. In this study, we will focus specifically on LGE-based scar identification for use in cardiac computational models.

Several methods have been described to identify scar tissue from LGE-cMRI, including image intensity ratio (IIR), standard deviation methods based on myocardial wall intensity (STD-wall) or blood pool intensity (STD-bp), and machine learning approaches.[3–7] Each method proposes a different ultimate threshold for scar in any given LGE-cMRI, leading to different scar patterns throughout the atria. This may also lead to different results from patient-specific computational model simulations. [2, 8] Automated methods seek to overcome limitations inherent to LGE-cMRI, and eschew human-mediated threshold selection, a reasonable choice to avoid human-induced biases. However, such approaches forgo the human ability to integrate supplemental information. For example, the location of ablation lesions from electro-anatomical mapping may guide a human-selected scar threshold in ways that other automated methods cannot easily incorporate.

In this study, we compared automated and human-guided left atrial scar identification methods in terms of both the distribution of scar tissue identified and the resulting computational modeling differences. We found that not only do automated methods differ substantially from humans in the identified scar distributions, but also that

each method yields substantially different simulation outcomes in terms of arrhythmogenic potential in simulated atria.

Table 1: Model parameter values. Target conductivities in the longitudinal σ_l, off axis (sheet and normal) σ_O directions given in m/s. Initial un-tuned intracellular conductivities (Longitudinal: g_{iL}, off-axis (sheet and normal): g_{iO}) are given in S/m. Tuning was performed on each mesh. Ionic conductivities given as factors[1] times the baseline values in the Courtemanche model.[9]

Parameter	Healthy Tissue	Fibrotic Tissue
CV_l (m/s)	0.8	0.32
CV_O(m/s)	0.4	0.16
g_{iL}	0.4	0.253
g_{iO}	0.107	0.0677
GKr	1.6	1.6
GNa	2	1.2
GK1	0.8	0.4
Gto	0.5	0.5
factorGKur	0.5	0.5
GCal	0.3	0.15

2. Methods

In this project we pursued two sub studies: 1) comparison of scar identification be different methods, and 2) comparison of simulated arrhythmogeneis using the identified scar distributions.

Model Generation and Arrhythmia Simulation: LGE-cMRI for 50 post-first-time atrial fibrillation left atrial radiofrequency ablation patients were collected from the University of Utah health record systems. Left atrial anatomy was identified using a combination of Seg3D (www.seg3d.org) and the automated pipeline CardioTwin (NumeriCor GmbH, Graz, Austria). Volumetric left atrial computational models (complete with rule-based fibers and universal atrial coordinates) were constructed at a target mesh resolution of both 250 μM and 750 μM average edge length as described previously [1, 10, 11]. Two separate mesh resolutions were produced to meet the needs of two sub studies: scar identification and simulation. During scar identification by human observers, the coarser mesh (750 μM) was used to reduce the computational demand of visualizing LGE-cMRI intensity and scar distributions in real time across multiple subjects. Subsequent computational modeling used a finer mesh (250 μM) to ensure accuracy of the simulations. Simulation of atrial electrophysiology was performed using the open-source simulation package openCARP via the monodomain formulation.[12] Ionic model and tissue parameters were prescribed according to table 1 as ratios of the original Courtemanche model. Iterative tuning of conductivities was used to achieve mesh-specific target conduction velocities shown in table 1.[1] Regional ionic heterogeneity was assigned according to Roney *et al.*.[1] This included additional scaling in the left appendage (GKr*1.6, GNa*2, GK1*0.8, GCaL*0.318, Gto*0.335, factorGKur*0.5) and pulmonary veins (Gto*0.375, GCaL*0.225, GKr*2.4, GKs*0.67, factorGKur*0.5). Scar was modeled as an extracellular bath with a conductivity of 0.05 S/m. Ionic models were prepaced for 1000 cycles at a cycle length of 500 ms. Prepaced cellular action potentials demonstrated stable APDs and shapes. Arrhythmia induction was simulated via two S1 pulses at 500 ms cycle length, followed by a burst of 10 stimuli. This protocol was repeated independantly for S2 burst cycle lengths ranging from 140 ms to 210 ms in 10 ms increments. Each of these 8 pacing protocols was repeated at 9 pacing sites defined across the left atrium using universal atrial coordinates, for a total of 72 pacing scenarios. Continued electrical activity at 2 seconds past the final pacing was considered an induced re-entrant arrhythmia.

Scar Identification Automated scar assessment was performed using each of the following: Image intensity ratio (IIR, scar threshold of 1.6), standard deviation of the wall (STD-wall, scar threshold of 3 standard deviations above mean), and standard deviation of the blood pool (STD-bp, scar threshold of 3 standard deviations above mean). We followed the implementation details outlined in the literature to derive the LGE-cMRI threshold for each patient for each automated scar identification method.[3–6] Human-guided scar identification consisted of allowing an expert to select the LGE threshold to classify the regions of the atria into scar and non-scar. Observers were shown the following for each case: the LGE intensity mapped to the 750 μM resolution atrial model, a histogram of the LGE intensity values, the anatomy and ablation tags from the patient's atrial ablation procedure, and an atrial geometry with a binary mask of scar and non-scar for the selected threshold. The experts could rotate both the LGE model and the ablation lesion model, and used a sliding scale to select the LGE intensity threshold that identified only dense scar related to atrial ablation. A total of four observers participated. Subjects were presented in random order. Observers were blinded to all other aspects of the study, including the threshold selected by the automated methods, MRI quality, ablation outcome, and simulation outcome.

In all methods (automated or human-guided), an LGE-cMRI intensity threshold was identified. The LGE-cMRI intensity was mapped from MRI image space onto both the coarse and fine meshes for each subject via median mapping to the mesh node from the centroid of the nearest 10 MRI image voxels. Median of 10 nearest voxel values was chosen as a balance between computational efficiency and reduction of the effect of registration and segmentation errors, which could erroneously include high-intensity struc-

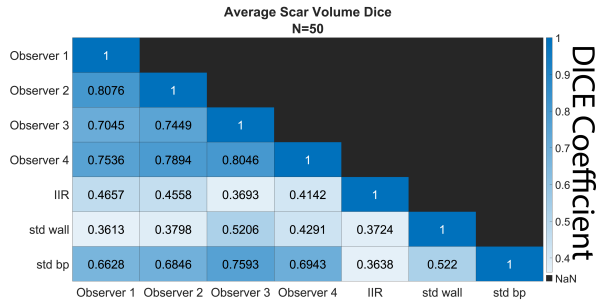

Figure 1: DICE coefficient of identified scar regions averaged over all 50 subjects. DICE of 1 (dark blue) indicates perfect overlap, and 0 (white) indicates no overlap.

tures near the left atrium, such as the aorta. All LGE intensity mappings were manually inspected, and segmentation or meshes were adjusted as needed to address noticeable mapping artifacts. Region identifiers were mapped from nodes to elements via integer median mapping of element node values.

To further reduce the effects of registration and segmentation errors of the myocardial wall (which is often only one or two voxels thick), we converted partial-thickness scars in the simulation meshes (250 μM resolution) into full transmural scars using the universal atrial transmural coordinate.

Scar comparisons Scar identification was compared using the DICE-Sørenson coefficient of scar volume between each method and/or observer using the 750 μM meshes. Additionally, simulations were run on a subset (4) of subjects as described above, one for each scar identification method or observer. The number of sustained re-entries observed in the simulations was compared across all scenarios. Scar patterns were also compared qualitatively via visual examination.

3. Results

We found that automated methods differed in the scar volumes they identified, both among themselves and when compared to human-guided scar identification. Human-guided scar identification was more consistent between observers. Figure 1 highlights the higher average agreement between human-to-human scar identifications (DICE scores above 0.7, often above 0.75). Human observers showed low average agreement with both IIR, and the STD-wall method (DICE below 0.52 on average), and slightly higher agreement with the STD-bp method (average DICE between 0.66 and 0.76). Figure 2 shows a single subject example in which the scar distribution is well matched between human subjects, and compared to humans, it is under-estimated in the IIR method, over-estimated in the STD-wall method, and slightly over-estimated in the STD-BP method.

Table 2: Number of re-entrant arrhythmias induced across all pacing scenarios for each scar identification method in four subjects.

Method	Subject 1	Subject 2	Subject 3	Subject 4
Observer 1	0	6	10	3
Observer 2	0	7	9	5
Observer 3	0	12	9	4
Observer 4	3	9	9	1
IIR	0	10	10	2
STD Wall	0	1	9	0
STD BP	3	10	11	1

Simulations were sensitive to scar distribution, showing differences in the number of arrhythmia events between scar identification methods as seen in Table 2. While some subjects showed higher (Subject 2 and 3) or lower (Subject 1 and 4) overall propensity for arrhythmia, there was no explicit agreement between identified scar patterns on the number of induced arrhythmias.

4. Discussion and Conclusions

We identified substantial disagreement between human and automated methods in identifying LGE-cMRI scar patterns, as well as high sensitivity in the downstream modeling of arrhythmogenesis to the selected scar pattern. Our results highlight the difficulty of producing robust and reliable patient-specific computational models for atrial fibrillation. LGE-cMRI is a standard input data modality for modeling studies, yet few explore the effects of process errors and uncertainties on the downstream modeling outputs.[8] In addition to the impact on simulated arrhythmogenesis of the models noted in these results, we also observed variability in the arrhythmia path and pattern across scar distributions, possibly impacting downstream use of the model to guide ablation procedures prospectively.

Numerous modeling assumptions and parameter choices in patient-specific computational models can influence reported simulation outcomes, underscoring the need for further uncertainty quantification and simulation studies. Future work will focus on characterizing and reducing model uncertainty while expanding the parameter space—such as incorporating fibrosis—to improve physiological realism. We will also investigate how variability in arrhythmia outcomes impacts the determination of optimal ablation strategies, helping assess the clinical reliability of these modeling approaches.

Acknowledgments

Support for this research came from the Center for Integrative Biomedical Computing (www.sci.utah.edu/cibc), NIH/NIGMS grants

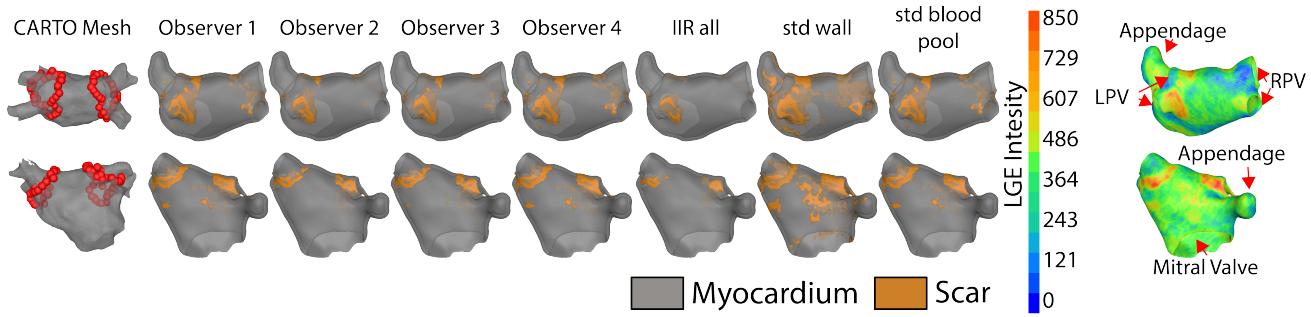

Figure 2: Comparison of identified scar regions across each observer or method.

P41 GM103545 and R24 GM136986, NIH/NIBIB grant U24EB029012, and the Nora Eccles Harrison Foundation for Cardiovascular Research. The support and resources from the Center for High Performance Computing at the University of Utah are gratefully acknowledged. The computational support of the Scientific Computing and Imaging Institute at the University of Utah are acknowledged. This work was supported by grant with Award Number 01CX002758-01 from the United States (U.S.) Department of Veterans Affairs CSRD Service.

References

[1] Roney CH, Bayer JD, Zahid S, Meo M, Boyle PM, Trayanova NA, Haïssaguerre M, Dubois R, Cochet H, Vigmond EJ. Modelling methodology of atrial fibrosis affects rotor dynamics and electrograms. Europace 2016;18(suppl 4):iv146–iv155.

[2] Orkild B, Bergquist JA, Paccione E, Lange M, Zenger B, Kwan E, Hunt B, MacLeod RS, Narayan A, Ranjan R. A grid search of fibrosis thresholds for uncertainty quantification in atrial flutter simulations. In 2023 Computing in Cardiology. 2023; 1–4.

[3] Hopman LHGA, Bhagirath P, Mulder MJ, Eggink IN, van Rossum AC, Allaart CP, Götte MJW. Quantification of left atrial fibrosis by 3D late gadolinium-enhanced cardiac magnetic resonance imaging in patients with atrial fibrillation: impact of different analysis methods. European Heart Journal Cardiovascular Imaging November 2021;23(9):1182–1190. ISSN 2047-2404.

[4] Khurram IM, Beinart R, Zipunnikov V, Dewire J, Yarmohammadi H, Sasaki T, Spragg DD, Marine JE, Berger RD, Halperin HR, Calkins H, Zimmerman SL, Nazarian S. Magnetic resonance image intensity ratio, a normalized measure to enable interpatient comparability of left atrial fibrosis. Heart Rhythm January 2014;11(1):85–92. ISSN 1547-5271.

[5] Benito EM, Carlosena-Remirez A, Guasch E, Prat-González S, Perea RJ, Figueras R, Borràs R, Andreu D, Arbelo E, Tolosana JM, Bisbal F, Brugada J, Berruezo A, Mont L. Left atrial fibrosis quantification by late gadolinium-enhanced magnetic resonance: a new method to standardize the thresholds for reproducibility. Europace August 2017;19(8):1272–1279. ISSN 1099-5129.

[6] Bertelsen L, Alarcón F, Andreasen L, Benito E, Olesen MS, Vejlstrup N, Mont L, Svendsen JH. Verification of threshold for image intensity ratio analyses of late gadolinium enhancement magnetic resonance imaging of left atrial fibrosis in 1.5T scans. The International Journal of Cardiovascular Imaging 2020;36(3):513–520. ISSN 1569-5794.

[7] Li L, Wu F, Yang G, Xu L, Wong T, Mohiaddin R, Firmin D, Keegan J, Zhuang X. Atrial scar quantification via multi-scale cnn in the graph-cuts framework. Medical image analysis 2020;60:101595.

[8] Bishop MJ, Plank G. Stochastic virtual heart model predictions. Nature Cardiovascular Research April 2025;1–4. ISSN 2731-0590. Publisher: Nature Publishing Group.

[9] Courtemanche M, Ramirez RJ, Nattel S. Ionic mechanisms underlying human atrial action potential properties: insights from a mathematical model. The American Journal of Physiology July 1998;275(1):H301–321. ISSN 0002-9513.

[10] Zappon E, Azzolin L, Gsell MAF, Thaler F, Prassl AJ, Arnold R, Gillette K, Kariman M, Manninger-Wünscher M, Scherr D, Neic A, Urschler M, Augustin CM, Vigmond EJ, Plank G. An efficient end-to-end computational framework for the generation of ECG calibrated volumetric models of human atrial electrophysiology, February 2025. URL http://arxiv.org/abs/2502.03322. ArXiv:2502.03322 [math].

[11] Bayer JD, Roney CH, Pashaei A, Jaïs P, Vigmond EJ. Novel radiofrequency ablation strategies for terminating atrial fibrillation in the left atrium: A simulation study. Frontiers in Physiology 2016;7:108. ISSN 1664-042X. URL https://www.frontiersin.org/articles/10.3389/fphys.2016.00108.

[12] Plank G, Loewe A, Neic A, Augustin C, Huang YL, Gsell MAF, Karabelas E, Nothstein M, Prassl AJ, Sánchez J, Seemann G, Vigmond EJ. The 'opencarp' simulation environment for cardiac electrophysiology. Computer Methods and Programs in Biomedicine 2021;208:106223. ISSN 0169-2607.

Address for correspondence:

Jake Bergquist
University of Utah
72 Central Campus Dr, Salt Lake City, UT 84112
jbergquist@sci.utah.edu